Observed Decline in Planetary Albedo and Recent Global Warming Acceleration

T. W. Patzek[1*]

[1]Professor Emeritus, Earth Sciences and Engineering Division, King Abdullah University of Science and Technology

Key Points:

- Planetary albedo derived from CERES observations declined after 2010 $\sim 0.37\%$ per decade, increasing absorbed shortwave radiation.
- The cumulative 2000–2024 top-of-atmosphere energy imbalance reached approximately 180 ZJ and increased more rapidly after 2014
- A simple energy-balance shows that the recent acceleration of global mean surface temperature tracks observed post-2010 albedo decline

[*]Current address, 4251 Norton Ave, Oakland, CA, 94602

Corresponding author: T.W. Patzek, tadeusz.patzek@kaust.edu.sa

Abstract

Recent satellite observations indicate that Earth's planetary albedo has declined since 2010, increasing solar-energy absorption by the climate system. Using CERES top-of-atmosphere radiative flux measurements, we estimate a mean albedo decline of $\sim 0.37\%$ per decade, corresponding to an additional absorbed shortwave flux approaching 1 $\mathrm{W\,m^{-2}}$. The associated cumulative heat uptake accelerated after 2014 and reached ~ 180 ZJ by 2024. We examine whether the observed albedo decline is dynamically consistent with the recent acceleration of global warming. A physically constrained energy-balance model combining greenhouse-gas radiative forcing with CERES-observed shortwave anomalies reproduces observed GMST evolution between 1880 and 2025 more closely than a greenhouse-gas-only baseline. The inferred attenuation timescale suggests substantial upper-ocean heat uptake during the CERES era. The observed post-2010 albedo decline appears energetically consistent with the post-2014 acceleration of GMST.

Plain Language Summary

Earth reflects part of the incoming sunlight back to space. This reflectivity, called planetary albedo, has declined since about 2010, allowing the Earth system to absorb more solar energy. Satellite observations from the CERES mission show that this decline accelerated after 2014 and was accompanied by rapidly increasing ocean heat uptake and rising global temperatures. Planetary albedo is not a fixed property of Earth. It changes together with the climate system through shifts in clouds, sea ice, water vapor, atmospheric circulation, aerosols, and ocean-atmosphere interactions such as El Niño. Because these processes are interconnected, some statistical methods used to remove short-term climate variability may also remove part of the underlying warming signal. We show that including satellite-observed albedo changes substantially improves agreement between modeled and observed global mean surface temperature from 1880 to 2025 compared with greenhouse-gas forcing alone. The results suggest that declining planetary albedo has become an important contributor to recent global warming.

1 Introduction

Recent years have seen a surge of record-breaking global temperatures and increasing evidence that global warming may be accelerating (Foster & Rahmstorf, 2011, 2026). Concurrently, anomalously warm subsurface waters have developed across the equatorial Pacific in 2026 (Figure S1), suggesting enhanced upper-ocean heat accumulation. This large-scale oceanic anomaly is used here only as qualitative supporting evidence for elevated ocean heat content, not as a basis for the statistical attribution developed below.

Further evidence for recent warming acceleration was presented by (Foster & Rahmstorf, 2026, FR26), who statistically separated the global surface air temperature signal from the effects of El Niño variability, volcanic aerosols, and solar forcing. However, their inference remains conditional on the statistical assumptions underlying the deconvolution and on the separation of internally generated variability from externally forced warming.

Mixed-baseline forcing and the albedo offset problem. The standard representation, e.g., Arias et al. (2021), of global-mean surface air temperature (GMST) change is a linear superposition of three time-dependent radiative forcing components,

$$\Delta T(t) = \lambda \left[5.35 \ln\left(\frac{c(t)}{c_{\mathrm{PI}}}\right) + \Delta F_{\mathrm{SW},\downarrow}(t) + \Delta F_{\mathrm{other}}(t) \right], \tag{1}$$

where c_{PI} is the preindustrial CO_2 concentration (typically 1850), $\Delta F_{\mathrm{SW},\downarrow}(t)$ denotes shortwave (albedo-related) solar forcing (see Eq. (S.1), and $\Delta F_{\mathrm{other}}(t)$ aggregates all re-

maining forcings (longwave greenhouse gases, aerosols, etc.). The IPCC AR6 assessment (WGI, Ch. 4 and 7) implies the climate feedback parameter

$$\lambda \approx 0.5\text{–}1.0 \text{ K}\,(\text{W m}^{-2})^{-1}, \tag{2}$$

corresponding to the equilibrium climate sensitivity $ECS \approx 2.0$–4.5 °C.

In practice, however, $F_{\text{SW},\downarrow}(t))$ is not referenced to the same baseline as the logarithmic CO_2 forcing. Observational estimates of planetary albedo and absorbed solar radiation are derived primarily from the satellite era (e.g., CERES), with anomalies typically defined relative to ∼2000–2010. This mismatch of reference states introduces an implicit inconsistency in Eq. (1).

Recent studies have shown that increased absorbed shortwave radiation contributed substantially to the recent rise in Earth's energy imbalance and to the record warmth of 2023 (Goessling et al., 2025, Loeb et al., 2021).

A consistent formulation requires explicit recognition of the mixed baselines. Writing the temperature response relative to a common preindustrial reference while retaining observational albedo anomalies yields

$$\Delta T(t) = \lambda \left[5.35 \ln\left(\frac{c(t)}{c_{1850}}\right) - \frac{S_\oplus}{4}\left(\alpha(t) - \bar{\alpha}\right) + F_{\text{offset}} \right], \tag{3}$$

where $S_\oplus$ is the solar constant, α is planetary albedo, and F_{offset} is a constant term that absorbs the unknown shortwave forcing between 1850, and the albedo reference period for $\bar{\alpha}$ is (∼2000–2010).

Without F_{offset}, Eq. (3) implicitly assumes that $\bar{\alpha}_{1850} = \bar{\alpha}_{2010}$, which is unjustified given known changes in aerosols, land use, cryosphere, and cloud fields over the industrial period. Hansen et al. (2023) acknowledge the role of declining albedo in global warming, but treat albedo change as either forcing (aerosols) or feedback (clouds), and avoid anchoring planetary albedo to preindustrial conditions.

Pre-satellite shortwave forcing components of F_{offset}. The planetary albedo term is observationally well constrained in the satellite era and contributes substantially to recent forcing trends. However, its historical baseline is not directly observed, and thus its integration into a preindustrial-referenced forcing framework necessarily introduces an unresolved offset. This mixed-baseline problem is generally avoided in the standard literature but becomes explicit in formulations such as Eq. (3).

The best-constrained component of historical shortwave (albedo-related) forcing is anthropogenic aerosol forcing. According to Arias et al. (2021) (WGI, Ch. 7), the effective radiative forcing (ERF) from aerosols over the industrial period (1750–2019) is

$$F_{\text{aer}} \approx -1.1 \text{ W m}^{-2}, \qquad \text{likely range: } [-1.7, -0.4] \text{ W m}^{-2}. \tag{4}$$

This forcing is dominated by shortwave processes – direct scattering and, more importantly, aerosol–cloud interactions that increase planetary reflectivity (cloud brightening). In the present framework, F_{aer} constitutes a negative contribution to the offset term F_{offset}, partially compensating greenhouse-gas forcing prior to the satellite era.

Land-use change (LUC) also contributes to planetary albedo through surface reflectivity changes. The IPCC AR6 assessment gives

$$F_{\text{LUC}} \approx -0.15 \text{ W m}^{-2}, \tag{5}$$

for the net brightening effect of croplands and managed landscapes replacing darker natural vegetation. Although small in magnitude, this contribution is directionally consistent with aerosol forcing and thus reinforces the negative component of F_{offset}.

In contrast, cryospheric changes (snow and sea-ice albedo) introduce a positive shortwave forcing:

$$F_{\text{cryo}} \sim +0.1 \text{ to } +0.3 \text{ W m}^{-2} \quad \text{by} \quad \sim 2000. \tag{6}$$

However, this term is poorly constrained prior to the satellite era (pre-1979), with reconstructions relying on sparse observations and model inference.

Implications. If the observed CERES-era decline in planetary albedo were extrapolated backward over the full industrial period, it would imply a positive shortwave offset that would need to be reconciled with the negative aerosol forcing assessed in AR6. This tension suggests that much of the observed albedo decline may be a relatively recent phenomenon.

Explicit introduction of F_{offset} exposes a lack of closure in the historical energy budget and forces reconciliation between model-derived effective radiative forcing (e.g., aerosols and land use) and observation-based constraints from CERES-era radiative fluxes.

2 Methods

All data sets used in this paper, together with the software employed to generate the figures, are described in the Data Availability Statement. We use the NASA CERES data set (Levitus et al., 2017, Loeb et al., 2018) to compute the top-of-atmosphere (TOA) planetary albedo, the Berkeley Earth data for the Global Mean Surface Temperature (GMST) anomaly, and the mixed ice-core and NOAA data for the CO_2 concentration records back to 1850. For at least 45 years, the CO_2 concentration in the atmosphere has been a quadratic function of time (Patzek, 2026b). Although CERES EBAF products are among the most carefully calibrated TOA flux data sets available, residual instrumental and intercalibration uncertainties remain, especially when estimating long-term trends from a relatively short satellite record. The three TOA radiative flux components and the raw albedo are shown in Figures S2 – S4.

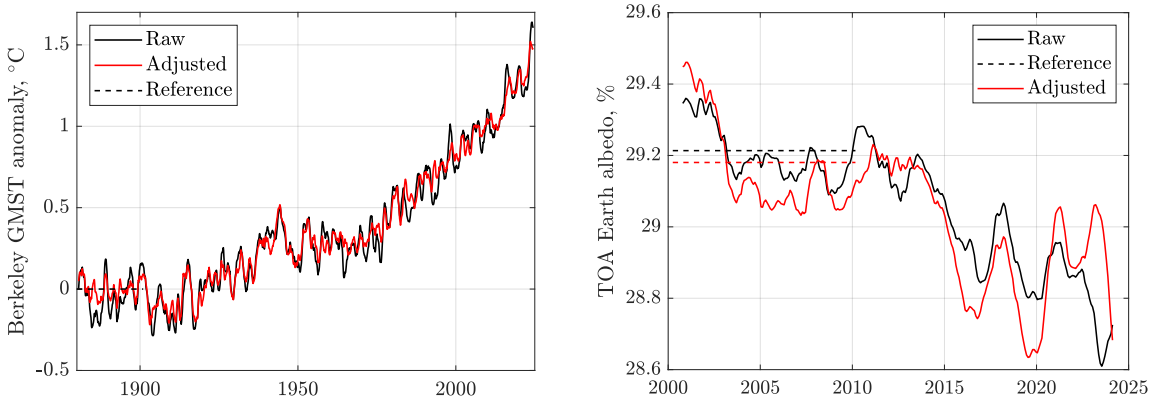

Figure 1: (**a**) Raw and adjusted Berkeley Earth Global Mean Surface Temperature (GMST) anomalies relative to the 1880-1900 average temperature of −0.3 °C. Note the thus shifted GMST anomaly was just shy of +1.5°C in 2024 and 2025. (**b**) The top of atmosphere (TOA) Earth albedo. The March 2000–Feb 2010 average albedo (≈ 29.2%) is the broken line.

A 12-month running mean of the albedo anomaly, defined relative to the 2000–2010 mean, and the corresponding absorbed shortwave flux are presented in Figure S5(top). The albedo-driven global cumulative heat uptake (CHU) is shown in Figure S5(bottom), together with ocean heat content (OHC) referenced to January 2000 to enable direct comparison of trends.

Following the pronounced post–March 2014 increase in slope, coincident with the acceleration of global warming reported by [FR26], the CHU curve exhibits a smaller magnitude (by ∼55 ZJ as of July 2024) but a steeper trend than the OHC curve. This divergence indicates that albedo-decline-driven CHU is becoming an increasingly important contributor to the ongoing accumulation of heat in the climate system.

The auxiliary data used to remove the effects of El Niño (ENSO3.4), volcanic aerosols, and solar variability from the CERES albedo signal are taken from the `ObservedData.csv` file distributed with [FR26]. The original R code was translated into MATLAB R24b and adapted for TOA albedo analysis because shortwave reflection is strongly modulated by ENSO through changes in marine stratocumulus, tropical convection, water vapor, and cloud cover (Allan & Liu, 2014, Trenberth & Caron, 2001). In addition, the inferred trend depends sensitively on the chosen start date and on whether ENSO, volcanic recovery, and solar-cycle variability are statistically removed (Deser et al., 2012, Foster & Rahmstorf, 2011). Since the CERES record is short and autocorrelated, ordinary least-squares confidence intervals may also be overly optimistic (Santer et al., 2000, Wilks, 2011).

At the same time, statistically adjusting the TOA albedo is physically nontrivial. A CERES-derived decline in reflected shortwave radiation represents a real change in the TOA energy budget, but it is not necessarily an external radiative forcing in the AR6 sense because part of the signal may arise from feedbacks or internally generated variability rather than from an imposed forcing (Gregory et al., 2004). Moreover, the CERES record spans only 2000–2024, far shorter than the temperature records analyzed by [FR26], making robust separation of secular trends from internal variability difficult. The statistical relationship between ENSO and planetary albedo therefore remains uncertain, and regression-based adjustments may inadvertently remove physically meaningful covariance or introduce spurious trends.

Following [FR26], we adopt an additive decomposition in which the albedo trend is represented by a smooth function of time, $g(t)$. Owing to the large heat capacity of the oceans and the inertia of sea-surface temperature (SST), $g(t)$ is expected to vary slowly and to be largely free of high-frequency fluctuations. The model is

$$x(t) = g(t) + c_V V_{k_1}(t) + c_N N_{k_2}(t) + c_S S_{k_3}(t) + \varepsilon(t). \tag{7}$$

Here, $V_{k_1}(t)$ denotes the volcanic aerosol optical depth (AOD) lagged by k_1 months, $N_{k_2}(t)$ is the NINO3.4 index (ENSO) lagged by k_2 months, and $S_{k_3}(t)$ is the total solar irradiance (TSI) lagged by k_3 months. The coefficients c_V, c_N, and c_S quantify the linear response to these forcings, while $\varepsilon(t)$ is a stationary residual process.

The coefficients and optimal lags (k_1, k_2, k_3) are estimated by ordinary least squares following [FR26].

3 Results

The raw and adjusted GMST and albedo records are plotted in Figure 1. The GMST reference temperature differs slightly from that used by [FR26], but the resulting adjustments are nearly identical. The lag intervals used for the GMST and albedo adjustments are 1950–2025 and 2000–2024, respectively. With this choice of lag interval, the albedo adjustment is substantial, yet it preserves both the reference albedo, $\bar{\alpha}$, in Eq. (S.6), and the total cumulative ocean heat uptake calculated from Eq. (S.8).

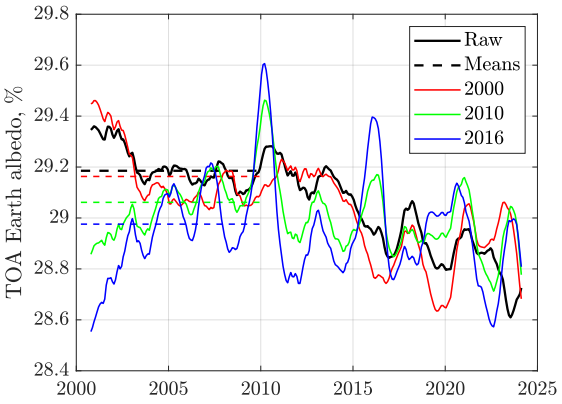

Figure 2: Twelve-month averages of the TOA albedo: the raw profile and three adjustments with the lag intervals starting in the year indicated by the legend. The reference means from 03/2000 to 2/2010 are shown as broken lines.

The sensitivity and instability of the albedo adjustment are illustrated in Figure 2. Only when the adjustment interval spans the full CERES record does the adjustment preserve the March 2000–February 2010 reference mean and yield a comparable cumulative absorbed heat anomaly. In contrast, the two alternative adjustments, initialized in February 2010 and January 2016, remain broadly in phase with one another, but differ substantially from the raw albedo trajectory and produce markedly different reference means.

Assuming that the adjusted GMST profile in Figure 1(a) provides a reasonable approximation to the forced temperature response, the next question is which of the two albedo trajectories shown in Figure 1(b) yields a better fit of Equation (3) to the adjusted GMST record. To address this question, Equation (3) is recast as a constrained three-parameter optimization problem,

$$
\begin{aligned}
\min_{x\in\mathcal{F}} = & \underbrace{\sum_{i\in\mathcal{B}} \left[GMST(t_i) - T_{\text{base}}(x_1, x_2, t_i)\right]^2}_{\text{Baseline CO}_2\text{−only model}} \\
& + \underbrace{\sum_{j\in\mathcal{C}} \left[GMST(t_j) - T_{\alpha}(x_1, x_2, x_3, t_j)\right]^2}_{\text{Albedo change perturbation}}, \qquad (8) \\
T_{\text{base}} = & \, x_1 \left(5.35 \ln\left(\frac{c(t_i)}{c_{1850}}\right) - 1.05 + x_2\right), \\
T_{\alpha} = & \, x_1 \left[5.35 \ln\left(\frac{c(t_j)}{c_{1850}}\right) - 1.05 + x_2 + x_3 \frac{S_{\oplus}}{4} \underbrace{\left(\alpha(t_j) - \bar{\alpha}\right)}_{\text{Polynomial fit}}\right], \\
& x = [x_1, x_2, x_3] = [\lambda, F_{\text{clouds,residual}}, \alpha_{\text{mult}}].
\end{aligned}
$$

Here, $\mathcal{B}$ denotes the set of monthly GMST observations between 1880 and 2025, while $\mathcal{C}$ denotes the subset of monthly records for which both GMST and CERES albedo data are available (2000–2024). The feasible set $\mathcal{F}$ imposes inequality constraints on the parameter vector x, consistent with Equation (2),

$$\begin{aligned} \lambda &\in [0.5, 1]\ \mathrm{K\,W^{-1}\,m^2}, \\ F_{\mathrm{clouds,residual}} &\in [0.5, 1.5]\ \mathrm{W\,m^{-2}}, \\ \alpha_{\mathrm{mult}} &\in [0.2, 1]. \end{aligned} \tag{9}$$

The constraint in Equation $(9)_3$ requires further explanation. It reflects the assumption that, over the relatively short CERES observation interval, the full magnitude of the TOA radiative imbalance cannot be instantaneously expressed in surface temperature because of the large heat capacity of the oceans and vigorous turbulent mixing within the upper ocean. Consequently, the surface-temperature response to albedo-driven forcing is expected to remain approximately in phase with the TOA signal, but attenuated in amplitude. The attenuation factor is represented here by a constant multiplier, α_{mult}, whose lower bound of 0.2 is necessarily heuristic.

3.1 Statistical procedure

The CO_2-only model represents the smooth greenhouse-gas-dominated warming trajectory using atmospheric CO_2 concentration as a compact proxy for the long-term anthropogenic forcing. It is not intended to reproduce the complete AR6 forcing decomposition, but rather to provide a deliberately parsimonious baseline against which the incremental explanatory power of CERES-observed shortwave anomaly can be tested. The combined aerosol and land-use-change (LUC) forcing is represented by a fixed offset of $-1.05\ \mathrm{W\,m^{-2}}$, while the remaining unresolved shortwave contribution is captured by the optimized parameter $F_{\mathrm{clouds,residual}}$. The corresponding optimal fit is shown in-Figure 3(top).

The albedo-augmented model additionally includes the effect of planetary albedo decline. Because the green baseline CO_2-only model temperature fit in Figure 3(top) is smooth, the raw CERES albedo anomaly in Figure 1(b) must also be replaced by a smooth polynomial approximation. Otherwise, high-frequency variability in the raw albedo record would bias the correlation analysis relative to the smooth CO_2-only fit.

This procedure is illustrated in Figure S6, where the raw CERES albedo anomaly is replaced by a smooth fitted curve (blue), making it statistically comparable to the smooth baseline CO_2-only model-fit (green). Both modeled temperature trajectories are then correlated against the reference GMST response (red), and the question becomes which model provides the statistically superior fit at the 95% confidence level.

The three time series are cross-correlated using Pearson linear correlation coefficients, r_{ij}, where $i, j = \mathrm{GMST, CO2, Albedo}$ and $i \neq j$. The dependent correlations are then compared using the Williams test Williams (1959). Because both GMST and CERES albedo records exhibit substantial temporal autocorrelation, effective sample sizes are smaller than the nominal monthly record length. Consequently, formal significance estimates should be interpreted cautiously.

The albedo-augmented model, which incorporates the observed decline in planetary albedo, exhibits a stronger correlation with GMST than the baseline CO_2-only model (Table S1).

However, repeating the same procedure with the statistically adjusted albedo anomaly shown in Figure 1(b) leads to rejection of the albedo-augmented models. The adjusted albedo fit correlates with GMST less strongly than the raw albedo fit. This result suggests that part of the variability removed during the statistical adjustment may represent physically meaningful covariance between planetary albedo and global warming, rather than purely exogenous noise.

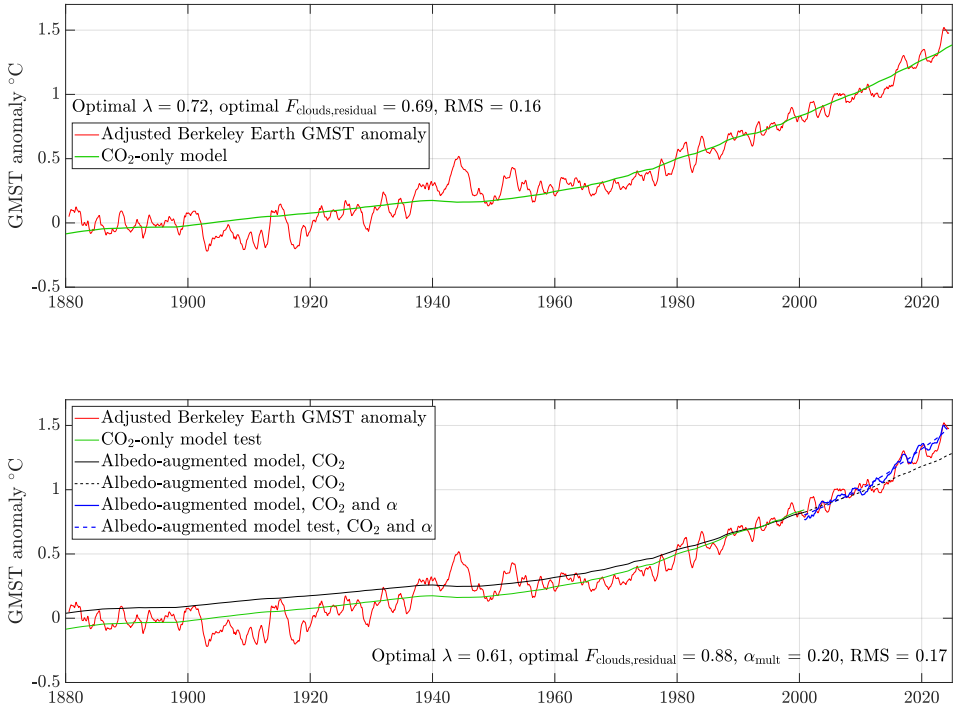

Figure 3: (**Top**) The CO_2-only model assumes that the GMST response is driven solely by the increasing atmospheric concentration of CO_2. (**Bottom**) The albedo-augmented model assumes that the GMST response is driven by the increasing atmospheric concentration of CO_2 and the decreasing raw albedo.

Figure 3(bottom) shows the optimal fit of the albedo-augmented model. The 12-month moving average of the raw CERES albedo anomaly (blue) is plotted together with its quadratic trend fit (broken blue curve). Interestingly, the CO_2-only temperature responses between 1880 and 2000 are statistically indistinguishable. Over this interval, the baseline CO_2-only model trajectory (green) lies slightly below the albedo-augmented model trajectory (black), but the corresponding Student's statistic satisfies $t \approx 0$. Thus, both temperature trends are effectively collinear with the observed GMST response and cannot be distinguished statistically over the 120 years of pre-CERES period. During 1880–2000, the root-mean-square (RMS) deviations of both hypotheses differ from GMST by $\mathcal{O}(10^{-1})$ °C.

4 Discussion

After 2000, the albedo-augmented model fits observed GMST significantly better than the greenhouse-gas proxy model alone. This is consistent with the interpretation that the recent warming acceleration may not be fully captured by increased longwave greenhouse trapping alone, but is also associated with enhanced absorption of incoming solar radiation as planetary albedo declines.

Since the adjusted GMST correlates more strongly with the raw albedo decline than with the adjusted albedo, several interpretations are possible: (i) the adjustment procedure removes physically meaningful covariance; (ii) ENSO partly mediates the albedo

Table 1: Optimal parameters for the baseline CO_2-only and albedo-augmented models of GMST response 1880–2025.

Hypothesis	Climate parameter λ	$F_{\text{clouds,residual}}$	α_{mult}
Baseline CO_2-only	0.72	0.69	n/a
Albedo-augmented	0.61	0.88	0.20

response rather than merely contaminating it; (iii) the Foster–Rahmstorf-style decomposition is overly simplistic for TOA albedo dynamics; or (iv) the raw albedo is strongly coupled to upper-ocean temperature, remains approximately in phase with the adjusted GMST, and its surface manifestation is damped to only $\sim 20\%$ of the TOA amplitude by oceanic low-pass filtering, reducing the physical interpretability of an ENSO adjustment. Among these possibilities, interpretation (iv) appears broadly consistent with the observed phase coherence between GMST and the raw CERES albedo anomaly.

A convenient representation of the climate system response to a changing albedo is the one-box energy-balance low-pass filter

$$C\frac{dT}{dt} + \frac{1}{\lambda}T = \Delta F_\alpha(t), \tag{10}$$

where C is the effective heat capacity of the upper ocean–climate system, λ is the climate feedback parameter, and $\Delta F_\alpha(t)$ is the time-dependent radiative forcing anomaly from albedo change. For an effective ocean depth of $H = 300$ m,

$$C = \rho_w c_p H \approx (1025)(3990)(300) \approx 1.23 \times 10^9 \ \mathrm{J\,m^{-2}\,K^{-1}}.$$

The impulse response of this system is exponential, with characteristic time constant

$$\tau = \lambda C. \tag{11}$$

For monthly forcing data $\Delta F_\alpha(t)$ in $\mathrm{W\,m^{-2}}$, a discrete-time recursion was implemented in MATLAB. Assuming $1/\lambda = 1.2\ \mathrm{W\,m^{-2}\,K^{-1}}$ (our best-fit value), the corresponding response times are approximately

$$\begin{aligned} H = 100\ \text{m} \quad &\Rightarrow \quad \tau \approx 10\ \text{yr}, \\ H = 300\ \text{m} \quad &\Rightarrow \quad \tau \approx 30\ \text{yr}, \end{aligned} \tag{12}$$

Increasing H mimics stronger coupling with the upper ocean and damps ENSO-scale variability more effectively.

Figure 4 summarizes the central result of this paper. The left panel shows the GMST anomaly driven by albedo-change forcing after attenuation by near-surface ocean water layers of different depths, ranging from 50 to 1000 m (Equation (10)). Also shown is the TOA raw albedo anomaly calculated from the second term in Equation (3) and scaled by α_{mult} from Table 1. The results suggest that the attenuation of the TOA forcing amplitude can be explained by heat transfer into the well-mixed upper ocean to a depth of up to 300 m, fully consistent with the timespan of the CERES observations.

The right panel shows the corresponding cumulative ocean heat uptake associated with the filtered CERES-observed shortwave anomaly for different ocean depths, together

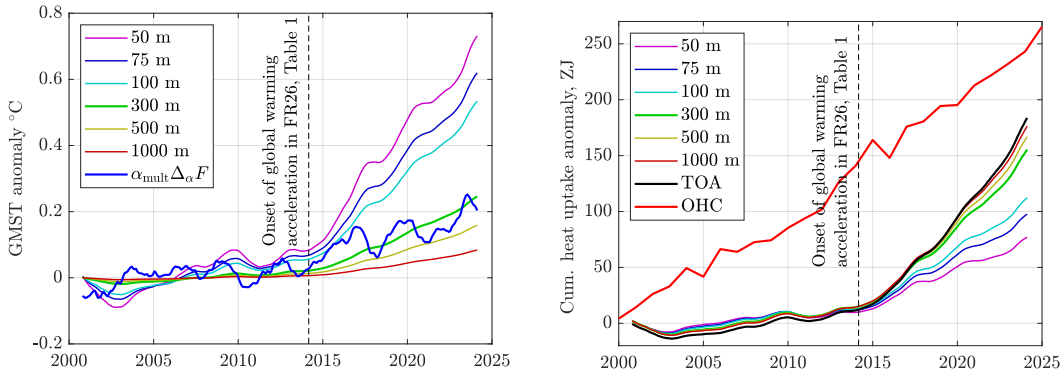

(a) (b)

Figure 4: (**a**) Modeled GMST response to observed planetary albedo decline for different effective upper-ocean depths. (**b**) Corresponding cumulative heat uptake anomalies compared with observed ocean heat content (OHC).

with the TOA cumulative heat uptake from Eq. (S.7). Over the 24-year CERES record, an ocean layer approximately 300 m deep absorbs most of the TOA $\Delta F_\alpha(t)$ forcing.

Notice the pronounced increase in the slope of cumulative heat uptake after 2014, emblematic of the acceleration of global warming associated with the post-2010 decline in planetary albedo. This result is consistent with the independent statistical analysis of GMST by [FR26], which identified a similar acceleration without invoking the CERES-observed shortwave anomaly. The present results are physically consistent with the statistical conclusions of [FR26].

Several limitations should be emphasized. First, the CERES record is short relative to multidecadal internal variability, so trend estimates remain sensitive to the chosen start date and statistical adjustment. Second, the albedo term combines forcing, feedback, and internally generated variability and therefore is not an external forcing in the strict AR6 effective-radiative-forcing sense. Third, the one-box upper-ocean filter is a deliberately reduced representation of ocean heat uptake. The result should therefore be interpreted as evidence that declining albedo is dynamically and energetically consistent with recent warming acceleration, not as a complete attribution of that acceleration.

Although planetary albedo is not an external forcing independent of climate, the observed post-2010 decline appears to contribute to and amplify ongoing global warming, and is energetically consistent with the post-2014 acceleration of GMST.

Conflict of Interest

The author declares no conflicts of interest relevant to this study.

Availability Statement

The input data and MATLAB software necessary to fully reproduce all calculations and figures in this paper are in Patzek (2026a), https://doi.org/10.5281/zenodo.20432638.

Acknowledgments

This work was supported by baseline funding to Prof. Patzek from KAUST.

References

Allan, R. P., & Liu, C. (2014). Changes in global net radiative imbalance 1985–2012. *Geophysical Research Letters*, *41*, 5588–5597. doi: https://doi.org/10.1002/2014GL060962

Arias, P., Bellouin, N., Coppola, E., Jones, R. G., Krinner, G., Marotzke, J., ... Zhou, B. (2021). Climate change 2021: The physical science basis. contribution of working group i to the sixth assessment report of the intergovernmental panel on climate change. *Intergovernmental Panel on Climate Change (IPCC)*. Retrieved from `https://www.ipcc.ch/report/ar6/wg1/` (Includes reference temperature periods such as 1850–1900 (pre-industrial) and 1995–2014 (modern baseline).) doi: https://doi.org/10.1017/9781009157896.002

Deser, C., Phillips, A. S., Bourdette, V., & Teng, H. (2012). Uncertainty in climate change projections: the role of internal variability. *Climate Dynamics*, *38*, 527–546. doi: https://doi.org/10.1007/s00382-010-0977-x

Foster, G., & Rahmstorf, S. (2011, dec). Global temperature evolution 1979–2010. *Environmental Research Letters*, *6*(4), 044022. Retrieved from `https://doi.org/10.1088/1748-9326/6/4/044022` doi: https://doi.org/10.1088/1748-9326/6/4/044022

Foster, G., & Rahmstorf, S. (2026). Global Warming Has Accelerated Significantly. *Geophysical Research Letters*, *53*(5), e2025GL118804. Retrieved from `https://agupubs.onlinelibrary.wiley.com/doi/abs/10.1029/2025GL118804` (e2025GL118804 2025GL118804) doi: https://doi.org/10.1029/2025GL118804

Goessling, H. F., Rackow, T., & Jung, T. (2025). Recent global temperature surge intensified by record-low planetary albedo. *Science*, *387*(6729), 68-73. Retrieved from `https://www.science.org/doi/abs/10.1126/science.adq7280` doi: https://doi.org/10.1126/science.adq7280

Gregory, J. M., Ingram, W. J., Palmer, M. A., Jones, G. S., Stott, P. A., Thorpe, R. B., ... Williams, K. D. (2004). A new method for diagnosing radiative forcing and climate sensitivity. *Geophysical Research Letters*, *31*(3), L03205. Retrieved from `https://doi.org/10.1029/2003GL018747` doi: https://doi.org/10.1029/2003GL018747

Hansen, J. E., Sato, M., Simons, L., Nazarenko, L. S., Sangha, I., Kharecha, P., ... Li, J. (2023). Global warming in the pipeline. *Oxford Open Clim. Change*, *3*(1), kgad008. doi: https://doi.org/10.1093/oxfclm/kgad008

Levitus, S., Antonov, J. I., Boyer, T. P., Baranova, O. K., García, H. E., Locarnini, R. A., ... Zweng, M. M. (2017). *NCEI ocean heat content, temperature anomalies, salinity anomalies, thermosteric sea level anomalies, halosteric sea level anomalies, and total steric sea level anomalies from 1955 to present calculated from in situ oceanographic subsurface profile data.* NOAA National Centers for Environmental Information. Retrieved from `https://doi.org/10.7289/v53f4mvp` (NCEI Accession 0164586) doi: https://doi.org/10.7289/v53f4mvp

Loeb, N. G., Doelling, D. R., Wang, H., Su, W., Nguyen, C., Corbett, J. G., ... Kato, S. (2018). Clouds and the earth's radiant energy system (ceres) energy balanced and filled (ebaf) top-of-atmosphere (toa) edition-4.0 data product. *Journal of Climate*, *31*(2), 895 - 918. Retrieved from `https://journals.ametsoc.org/view/journals/clim/31/2/jcli-d-17-0208.1.xml` doi: 10.1175/JCLI-D-17-0208.1

Loeb, N. G., Johnson, G. C., Thorsen, T. J., Lyman, J. M., Rose, F. G., & Kato, S. (2021). Satellite and Ocean Data Reveal Marked Increase in Earth's Heating Rate. *Geophysical Research Letters*, *48*(13), e2021GL093047. Retrieved from

https://agupubs.onlinelibrary.wiley.com/doi/abs/10.1029/2021GL093047 doi: https://doi.org/10.1029/2021GL093047

Patzek, T. W. (2026a). *MATLAB Code and Data for Method of Patzek (2026)* [Dataset]. Zenodo. Retrieved from https://zenodo.org/uploads/20432638 ([Dataset] [Software]) doi: https://doi.org/10.5281/zenodo.20432638

Patzek, T. W. (2026b). *Thermal power and climate change: A data-driven analysis of cause and effect, 1800–2100.* EarthArXiv preprint. Retrieved from https://doi.org/10.31223/X5PX7K doi: https://doi.org/10.31223/X5PX7K

Santer, B. D., Wigley, T. M. L., Boyle, J. S., Gaffen, D. J., Hnilo, J. J., Nychka, D., ... Taylor, K. E. (2000). Statistical significance of trends and trend differences in layer-average atmospheric temperature time series. *Journal of Geophysical Research: Atmospheres*, *105*(D6), 7337–7356. doi: https://doi.org/10.1029/1999JD901105

Trenberth, K. E., & Caron, J. M. (2001). Estimates of Meridional Atmosphere and Ocean Heat Transports. *Journal of Climate*, *14*(16), 3433–3443. doi: https://doi.org/10.1175/1520-0442(2001)014⟨3433:EOMAAO⟩2.0.CO;2

Wilks, D. S. (2011). *Statistical Methods in the Atmospheric Sciences* (3rd ed., Vol. 100). Amsterdam, Netherlands: Academic Press. doi: https://doi.org/10.1016/C2009-0-60344-1

Williams, E. J. (1959). The Comparison of Regression Variables. *Journal of the Royal Statistical Society. Series B (Methodological)*, *21*(2), 396–399. doi: https://doi.org/10.1111/j.2517-6161.1959.tb00346.x